4562–4569 *Nucleic Acids Research, 1997, Vol. 25, No. 22*

Placement of the α-sarcin loop within the 50S subunit: evidence derived using a photolabile oligodeoxynucleotide probe

Parimi Muralikrishna[+], Rebecca W. Alexander[§] and Barry S. Cooperman*

Department of Chemistry, University of Pennsylvania, Philadelphia, PA 19104-6323, USA

Received July 25, 1997; Revised and Accepted October 1, 1997

ABSTRACT

We report the synthesis of a radioactive, photolabile oligodeoxyribonucleotide probe and its exploitation in identifying 50S ribosomal subunit components neighboring the α-sarcin loop. The probe is complementary to 23S rRNA nt 2653–2674. Photolysis of the complex formed between the probe and 50S subunits leads to site-specific probe photo-incorporation into proteins L2, the most highly labeled protein, L1, L15, L16 and L27, labeled to intermediate extents, and L5, L9, L17 and L24, each labeled to a minor extent. Portions of each of these proteins thus lie within 23 Å of nt U2653. These results lead us to conclude that the α-sarcin loop is located at the base of the L1 projection within the 50S subunit. Such placement, near the peptidyl transferase center, provides a rationale for the extreme sensitivity of ribosomal function to cleavage of the α-sarcin loop.

INTRODUCTION

The cytotoxin α-sarcin is a 17 kDa basic protein secreted by the fungus *Aspergillus giganteus* which is toxic to eukaryotic organisms. It inactivates the ribosomes of all species tested to date by cleaving a single phosphodiester bond within large subunit rRNA (1,2), despite the general tolerance of rRNA strand breaks elsewhere (3,4). This specific cleavage site, following G2661 in 23S rRNA, defines the α-sarcin stem–loop region, stretching from C2646 to G2674 (*Escherichia coli* numbering) (5). It contains the longest universally conserved sequence among rRNAs, corresponding in 23S rRNA to nt 2654–2665 (6; Fig. 1). Cleavage of the α-sarcin loop by α-sarcin or depurination of A2660 by the cytotoxin ricin inhibits factor-dependent steps of the elongation cycle (7,8), implying that the elongation factors interact with the α-sarcin domain. Indeed, both of the procaryotic factors EF-Tu and EF-G footprint at nucleotides within the α-sarcin loop (9; Fig. 1) and EF-G bound to the 50S subunit in the presence of fusidic acid protects the ribosome from α-sarcin inactivation (10). Results obtained with 23S rRNA variants suggest that the α-sarcin loop is also important for translational accuracy. Thus mutations at G2661 cause growth inhibition or cell death in strains with hyperaccurate S12 variants, reduce frameshifting and read-through of nonsense codons and show decreased sensitivity to drugs that impair proofreading control (11–14).

It has been proposed, based on *in vitro* mutational studies, that the α-sarcin loop alternates between an open 17 nt loop and a closed tetraloop and that these two conformations may drive the elongation cycle in response to binding of different elongation factors (15–17). An oligonucleotide model of the α-sarcin loop adopts a tetraloop conformation in solution, as determined by NMR spectroscopy and molecular dynamics simulations (18). This tetraloop structure, containing several non-canonical base pairs and a bulged G nucleotide at the position equivalent to 23S G2655, seems to provide the scaffolding necessary for elongation factor binding as well as toxin recognition. Thus mutations at the bulged G eliminate cleavage by α-sarcin, while insertion of extra nucleotides shifts the site of cleavage, indicating that the toxin cleaves a phosphodiester bond at a fixed distance from the bulged G (19). Evidence that the tetraloop conformation is at least transiently necessary comes from *in vivo* studies of yeast 25S rRNA, in which a mutation preventing closure of the tetraloop (at the position corresponding to 23S C2658) slowed cell growth, caused nonsense suppression and increased antibiotic resistance (20). In addition, C2666U and A2654G variants, which increase the stability of a non-canonical base pair in the α-sarcin loop, exhibited increased stop codon read-through and frameshifting (21).

We have been using radioactive photolabile oligoDNA probes targeted toward functionally important regions of rRNA to identify the ribosomal components that neighbor these rRNA regions (22–26) as an important step in the construction of three-dimensional models of ribosome structure and function (27). Given its importance for ribosomal function, the α-sarcin region is a prime candidate for such studies. Moreover, it has been shown to be accessible to complementary oligoDNAs within 70S ribosomes, as shown by the ability of these oligoDNAs to protect against α-sarcin cleavage of 23S rRNA (28).

Here we present experiments using the photolabile oligoDNA probe *N*-[5-hydroxymethyl-6-(3′-pATCATGCTCTCCTGGCCTC-ACCp*)]hexyl-*p*-azidobenzamide (p*2674–2653HHABA; Fig. 2), complementary to 23S rRNA nt 2674–2653 in the α-sarcin region, to identify ribosomal components within 23 of U2653. As seen in

*To whom correspondence should be addressed. Tel: +1 215 898 6330; Fax: +1 215 898 2037; Email: cooprman@pobox.upenn.edu

Present addresses: [+]Professional Access Ltd, 100 Wall Street, New York, NY 10005, USA and [§]The Skaggs Institute for Chemical Biology, The Scripps Research Institute, 10550 North Torrey Pines Road, La Jolla, CA 92037, USA

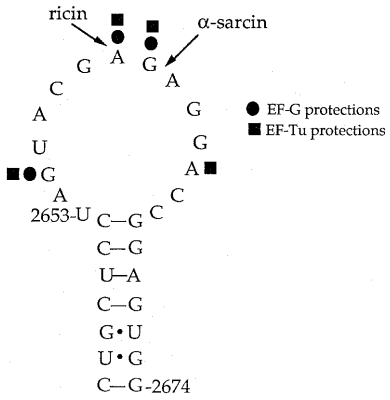

Figure 1. The α-sarcin loop of 23S rRNA. Sites of action are indicated for the ribosome-inactivating proteins α-sarcin, which cleaves the phosphodiester bond between G2661 and A2662, and ricin, which depurinates A2660. Nucleotides in the α-sarcin loop are protected from chemical modification in the presence of EF-G and EF-Tu as indicated. Modified from Moazed *et al.* (9). The NMR structure of a 29 base oligonucleotide containing a 23 nt sequence identical with the α-sarcin loop in rat 28S rRNA has a longer stem than that depicted, capped by a tetraloop GAGA corresponding to nt 2659–2662 (18).

Figure 2, the maximum distance between the nitrene generated upon photolysis of 2674–2653HHABA and the amine nitrogen of the 3′-terminal adenosine is 21 Å; the corresponding distance between the nitrene and the 4-oxygen of U2653 is 23 Å.

MATERIALS AND METHODS

Materials

Except as specified below, all materials were obtained as described (23–26).

Synthesis and purification of oligodeoxyribonucleotides. cDNA 2674–2652, having the sequence 5′-CCACTCCGGTCCTCTC-GTACTAG-3′, and the corresponding mismatched oligonucleotide 5′-CCAC**A**CCGGT**A**CTCTC**CA**ACTAG-3′ (MM-cDNA 2674–2652; mismatches with the target sequence in bold) were synthesized using phosphoramidite chemistry on a Milligen Biosearch Cyclone automated DNA synthesizer and deblocked according to the manufacturer's protocol. The photolabile 3′-*O*-(6-amino-2-hydroxymethyl)hexyl-*N*-*p*-azidobenzoate probe complementary to 23S nt 2653–2674 was synthesized as follows. 3′-Amino-modifier C7 CPG [(1-dimethoxytrityloxy-6-fluorenylmethoxycarbonylamino-hexane-2-methyl-*O*-succinyl) long chain alkylamino CPG] was used to generate cDNA 2674–2653 derivatized at its 3′-end with a primary amine according to the protocol supplied by Glen Research (Sterling, VA). After deblocking and RP-HPLC purification the 3′-amino-derivatized cDNA 2674–2653 was reacted with *N*-hydroxysuccinimidyl-4-azidobenzoate (HSAB) to yield 2674–2653HHABA, using a procedure described earlier (24). The photolabile derivative was purified from residual underivatized material by RP-HPLC using an acetonitrile gradient. The photolabile probe was radiolabeled at the 5′-end with [γ-^{32}P]ATP using polynucleotide kinase (29) to produce p*2674–2653HHABA. cDNA 2674–2652 labeled at its 5′-end, p*2674–2652, was prepared similarly. Radiolabeled oligoDNA probes and primers were purified using Sep-Pak C-18 cartridges (29).

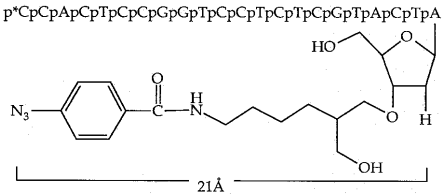

Figure 2. Photoaffinity probe 2674–2653HHABA. The distance between the photogenerated nitrene and the amine N of the nearest adenosine was determined to be 21 Å by molecular modeling with Quanta4.1 (Molecular Simulations Inc.).

Methods

The following methods were carried out as described (23–26): Millipore filter binding assay of non-covalent probe–subunit complex formation, localization of photoincorporation sites within 23S rRNA by RNase H and reverse transcriptase analyses. Proteins were prepared from labeled 50S subunits by acetic acid extraction and acetone precipitation in the usual fashion (30). Labeled proteins were identified by RP-HPLC (31), SDS–PAGE coupled with autoradiography (24–26) and, as needed, agarose antibody affinity chromatography (32).

*Photoincorporation of p*2674–2653HHABA into 50S subunits.* In a typical experiment 150 pmol 50S subunit were incubated with 20 pmol p*2674–2653HHABA in 100 µl TKM0.3 (50 mM Tris–HCl, pH 7.6, 50 mM KCl, 0.3 mM $MgCl_2$) at 37°C for 10 min and left on ice for 15 min. The $MgCl_2$ concentration was then increased to 10 mM and incubation was continued for an additional 2 h at 4°C. The reaction mixtures were layered on a 5–30% sucrose gradient containing TKM10 (50 mM Tris–HCl, pH 7.6, 50 mM KCl, 10 mM $MgCl_2$) buffer. Centrifugation was carried out at 4°C in a Beckman VTi80 rotor for 48 min at 50 000 r.p.m. Fractions containing the 50S subunit–p*2674–2653HHABA complex were pooled and subjected to photolysis with 3000 Å lamps (Rayonet) for 3 min as described (24). In a separate experiment sucrose was removed by ethanol precipitation and the 50S complex was redissolved in TKM10 buffer and photolyzed. No difference in the labeling pattern was observed for photolysis in the presence or absence of sucrose.

*Separation of p*2674–2653HHABA probe from labeled 50S rRNA.* Labeled 50S rRNA, prepared by phenol/chloroform extraction of labeled 50S subunits, was boiled for 3 min in 30% formamide/bromophenol blue/xylene cyanol running buffer prior to loading on a 4% acrylamide/0.2% bis(acrylamide)/7 M urea/TBE gel preheated to 50–55°C by application of a 20–40 mA current. The electrode buffer temperature was maintained at 50–55°C during electrophoresis. TBE is 89 mM Tris–borate, pH 8.3, 8 mM EDTA.

Preparation of 50S subunit rRNA as a substrate for reverse transcriptase. rRNA (100 pmol) was prepared from 50S subunits (either non-covalently complexed with cDNA 2674–2652 or photolabeled with p*2674–2653HHABA) by phenol/chloroform extraction, ethanol precipitation and digestion with 50 U RNase-free DNase I (Boehringer-Mannheim) in 0.1 M NaOAc, pH 5.2, 5 mM $MgCl_2$ (total volume, 200 µl) for 2 h at room temperature. The treated RNA was again phenol/chloroform extracted, ethanol precipitated and stored in 1 mM EDTA at –80°C.

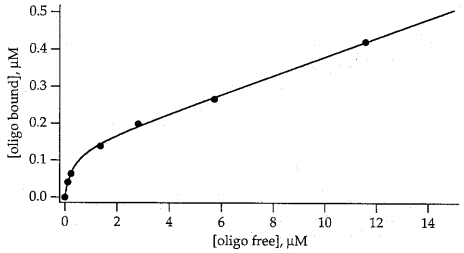

Figure 3. Millipore filter binding analysis of p*2674–2652 fitted to a two-population model. 50S subunits (15 pmol) were incubated with varying amounts of p*2674–2652 (300–500 c.p.m./pmol) and bound to Millipore filters as described (24). The amount of filter-bound oligonucleotide was determined by liquid scintillation counting of the dried filters. The total concentration of 50S subunits in the binding mix was 0.6 μM. The concentration of free oligo in the binding reaction is estimated from the difference in total (added) oligo concentration and bound oligo measured by counting the filters.

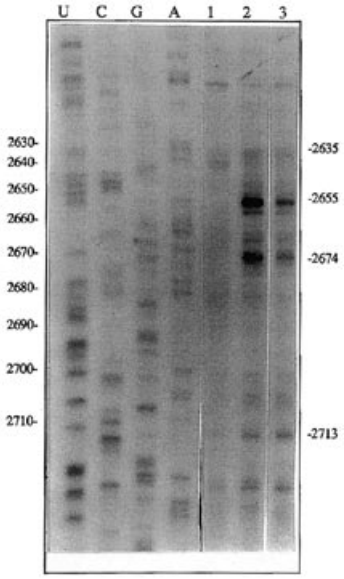

Figure 4. Primer extension analysis of DMS-treated 23S rRNA. 50S subunits (150 pmol) were modified with 1 μl DMS in the absence or presence (750 pmol) of cDNA 2674–2652 or 2674–2653HHABA in 30 mM potassium cacodylate, pH 7.2, 0.3 M KCl, 20 mM MgOAc (total volume 300 μl). Phenol:chloroform-extracted, ethanol-precipitated modified 23S rRNA (~100 pmol) was treated with DNase I (50 U) in 0.1 M NaOAc, pH 5.2, 5 mM $MgCl_2$ (total volume 200 μl) and re-extracted and precipitated prior to primer extension. Lane 1, DMS-modified 23S rRNA; lanes 2 and 3, in the presence of cDNA 2674–2652 or 2674–2653HHABA respectively. Lanes labeled U, C, G and A are sequencing products generated in the presence of ddATP, ddGTP, ddCTP and ddTTP respectively with 23S rRNA extracted from unmodified 50S subunits. Nucleotides at which pauses or stops are observed are indicated

RESULTS

Non-covalent binding of cDNAs directed to the α-sarcin region

Non-covalent binding of cDNA p*2674–2652 to 50S subunits was determined using a Millipore filter binding assay (Fig. 3). The results obtained, which are similar to those reported earlier for oligoDNAs directed to the α-sarcin loop (28), are consistent with a two population binding model, as described by equation **1**. Here L is the concentration of oligoDNA, a is the tighter binding fraction of the total amount of 50S subunits, R_t, and α is the weaker binding fraction. The two populations bind oligoDNA with apparent dissociation constants K_{app1} and K_{app2} respectively.

$$\text{bound} = aR_tL[(1/K_{app1} + L) + (\alpha/K_{app2} + L)] \qquad \mathbf{1}$$

Fitting the data in Figure 3 to this model yields the following parameter values: K_{app1}, 0.30 ± 0.06 μM; a, 0.22 ± 0.01; α/K_{app2}, 0.042 ± 0.004/μM. Thus ~20% of the 50S subunits bind cDNA 2674–2652 with high affinity.

Structural integrity of 50S subunits in the presence of non-covalently bound oligoDNA probe

To assess possible conformational changes resulting from non-covalent binding of probe oligoDNA to the α-sarcin stem–loop region (33,34), 50S subunits were treated with dimethyl sulfate (DMS) in the absence or presence of either cDNA 2674–2652 or 2674–2653HHABA. 23S rRNA prepared from such subunits was then examined as substrate in a reverse transcriptase primer extension assay using primers directed to nt 858–875, 1171–1187, 2100–2116, 2560–2576, 2781–2797 and 2888–2904. The presence of oligoDNAs was observed not to affect the DMS modification pattern except in the immediate vicinity of the α-sarcin stem–loop (Fig. 4). Enhanced reverse transcriptase stops were observed at nucleotides within the target site (2652–2674), which is likely due to incomplete removal of the oligoDNA by DNase I treatment. However, several enhanced stops outside the target site, at nt A2635 and U2713, indicated a probe-induced local unfolding of the 23S rRNA.

Overall binding and photoincorporation of p*2674–2653HHABA

Using the program Amplify (Bill Engels, University of Wisconson), overlapping 8mers within cDNA 2674–2653 were examined for complementarity to 23S rRNA. Excluding matching stretches in exclusively helical regions (35), the longest matches were: a 6 nt match at 520–525; a 5 nt match at 410–414; a 4 nt match at 1631–1634; 5 of 6 nt in a single-stranded region at 2223–2228. Photoincorporation experiments were designed to eliminate or minimize labeling of ribosomal components by p*2674–2653HHABA from such non-target sites, as well as to maximize binding to the tighter binding 50S population (Fig. 3). Accordingly, 50S–p*2674–2653HHABA complex was formed in a solution containing 50S subunits in stoichiometric excess over probe (typically 7.5-fold) and isolated by sucrose gradient centrifugation prior to photolysis. This ensures that photo-incorporation is dominated by the probe bound to its target site, since non-covalent binding to secondary sites would not be expected to survive sedimentation through a gradient. The probe–50S complex sedimented in approximately the same position on the sucrose gradient as did uncomplexed 50S subunits.

Table 1. Binding and photoincorporation of p*2674–2653HHABA[a]

Sample[b]	50S (binding)[c]	23S (photoincorporation)[d]	TP50 (photoincorporation)[e]
Standard	13	2	0.7
Pre-photolyzed	6	0.06	n.d.[f]
Standard + cDNA 2652–2674[g]	4	0.5	0.2
Standard + MM-cDNA 2652–2674[g]	11	2	0.7

[a]Numbers shown are pmol p*2674–2653HHABA.
[b]In the standard experiment 150 pmol 50S subunits and 20 pmol p*2674–2653HHABA were mixed, the non-covalent complex was isolated by sucrose gradient centrifugation and then photolyzed. In the pre-photolyzed control p*2674–2653HHABA was photolyzed prior to mixing with 50S subunits and there was no subsequent photolysis.
[c]Estimated from radioactivity co-sedimenting with 50S subunits on sucrose gradient centrifugation.
[d]Estimated from radioactivity co-migrating with 23S rRNA on urea–PAGE analysis.
[e]Total protein from 50S subunits. Estimated from radioactivity eluting with 50S protein on RP-HPLC analysis.
[f]Not determined. However, SDS–PAGE and autoradiographic analysis of TP50 from the pre-photolyzed sample showed negligible protein labeling.
[g]1125 pmol was added to the standard reaction mixture prior to sucrose gradient centrifugation.

Approximately 65% of probe mixed with excess 50S subunits was non-covalently bound to subunits following centrifugation (Table 1). Evidence that such binding was directed mainly toward the target site was provided by the large reduction in such binding (down to 20%) seen in the presence of cDNA 2674–2652, the unmodified oligoDNA which competes with the probe for binding to the target site. In contrast, only a slight reduction in binding (to 55%) was observed in the presence of MM-cDNA 2674–2652, designed to not compete for target site binding. Because of the length of the oligoDNA probe used in these experiments, mismatched bases were placed at three loci, corresponding to nt 2670, 2664 and 2657–2658, thus leaving no more than five contiguous nucleotides available for base pairing with the α-sarcin region.

The isolated non-covalent subunit–probe complexes were photolyzed as described in Materials and Methods, giving the incorporation yields summarized in Table 1. Approximately 20% of the non-covalently bound probe is photoincorporated into the 50S subunit, with incorporation into 23S RNA accounting for 75% of the total. Probe photoincorporation into 23S rRNA was determined by quantifying the radioactivity co-migrating with 23S rRNA on urea–PAGE analysis, which fully resolves free oligoDNA probe from 23S rRNA (Fig. 5A). No radioactivity migrated in the range 120–145 nt, ruling out appreciable labeling of 5S RNA. Probe photoincorporation into total protein from 50S subunits (TP50) was determined by summing the radioactivity co-eluting with TP50 on RP-HPLC analysis (see Fig. 7).

The negligible photoincorporation observed when p*2674–2653HHABA was pre-photolyzed prior to incubation with 50S subunits (Table 1) demonstrates the covalent nature of the labeling achieved on photolyzing the 50S–p*2674–2653HHABA complex. Paralleling the results for non-covalent binding, added cDNA 2674–2652 decreased photoincorporation to a much greater extent than added MM-cDNA 2674–2652. Labeled nucleotides and proteins were identified as described below.

Localization of p*2674–2653HHABA photoincorporation sites in 23S rRNA

RNase H cleavage of labeled 23S rRNA hybridized with various cDNAs, followed by PAGE and autoradiographic analysis of the products, allowed partial localization of probe photoincorporation. The apparent sizes of labeled fragments are typically larger (25–35 nt) than would be expected for the corresponding unlabeled fragments generated upon complete RNase H digestion due to both the size of the covalently bound probe and the multiple sites of

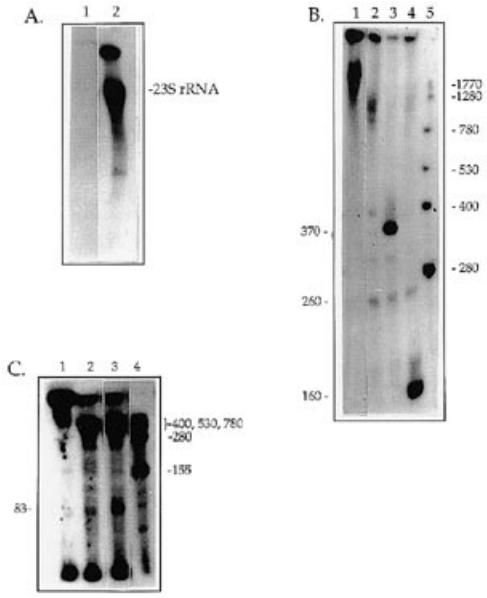

Figure 5. Identification of labeled sites within 23S rRNA by autoradiography. (**A**) Separation of p*2674–2653HHABA probe from labeled 23S rRNA by urea–PAGE analysis. Samples shown are for RNA from: 50S subunits incubated with pre-photolyzed p*2674–2653HHABA (lane 1); 50S subunits photolabeled with p*2674–2653HHABA (lane 2). (**B**) Partial localization of sites of photoincorporation into 23S rRNA using RNase H digestion. Labeled rRNA, purified from p*2674–2653HHABA-labeled 50S subunits by denaturing urea/SDS/LiCl/sucrose gradient centrifugation, was incubated with the indicated cDNA probe and digested with RNase H. The fragments were electrophoresed on a 5% polyacrylamide/0.25% bis(acrylamide) gel made up in 7 M urea, TBE. Lane 1, labeled 23S rRNA, incubated in the absence of RNase H. Lanes 2–4 were all digested with RNase H. Lane 2, no added cDNA; lane 3, with cDNA 2310–2301; lane 4, with cDNA 2505–2497; lane 5, RNA size markers, with sizes (nt) indicated to the right of the gel. Sizes to the left of the gel correspond to approximate sizes of labeled fragments produced by RNase H cleavage. (**C**) Further partial localization of sites of photoincorporation into 23S rRNA using RNase H digestion. Lane 1, labeled 23S rRNA incubated in the absence of RNase H. Lanes 2–4 were all digested with RNase H. Lane 2, no added cDNA; lane 3, with cDNA 2740–2731; lane 4, RNA size markers, with sizes (nt) indicated to the right of the gel. The fragments were electrophoresed on an 8% polyacrylamide/0.4% bis(acrylamide) gel made up in 7 M urea, TBE.

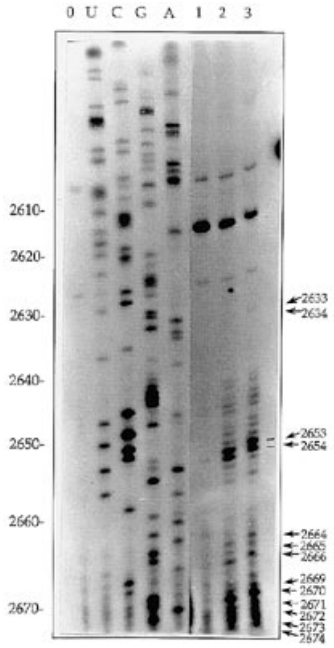

Figure 6. Reverse transcriptase analysis of 2674–2653HHABA-labeled 23S rRNA. Photoincorporation was carried out on a reaction mixture containing 150 pmol 50S subunits and 2674–2653HHABA in a total volume of 100 µl. Labeled 23S rRNA was treated with DNase I prior to the transcriptase assay. The primer used was cDNA 2697–2681. Lane 1, 23S rRNA extracted from 50S subunits photolyzed in the absence of 2674–2653HHABA; lane 2, rRNA extracted from 50S subunits photolyzed in the presence of 750 pmol 2674–2653HHABA; lane 3, rRNA extracted from 50S subunits photolyzed in the presence of 1500 pmol 2674–2653HHABA. Lanes labeled U, C, G and A are sequencing products generated in the presence of ddATP, ddGTP, ddCTP and ddTTP respectively with 23S rRNA extracted from unlabeled 50S subunits. Numbered nucleotides on the right correspond to positions at which pauses or stops dependent upon covalent incorporation of 2674–2653HHABA are observed.

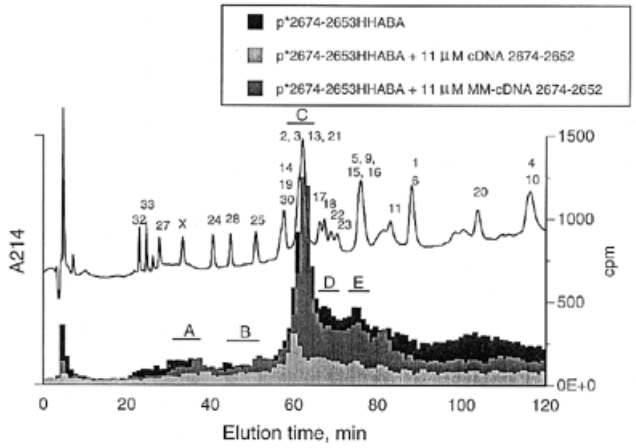

Figure 7. RP-HPLC analysis of labeled TP50. TP50 from photolyzed complexes of 50S subunits with p*2674–2653HHABA prepared in the absence or presence of cDNA 2674–2652 or MM-cDNA 2674–2652 were applied to a SynChropak RP-P reverse phase C18 column and eluted with the following gradient in the presence of 0.1% TFA, 0.7 ml/min: 15% ACN for 10 min, 15–45% ACN for 120 min (Perkin Elmer Series 4 convex curve 0.2); 45–75% ACN for 30 min (linear). Complexes were prepared by incubation of 50S subunits (150 pmol) and p*2674–2653HHABA (20 pmol) in the absence or presence (1125 pmol) of cDNA 2674–2652 or MM-cDNA 2674–2652 in a total volume of 100 µl and isolated by sucrose density gradient centrifugation prior to photolysis.

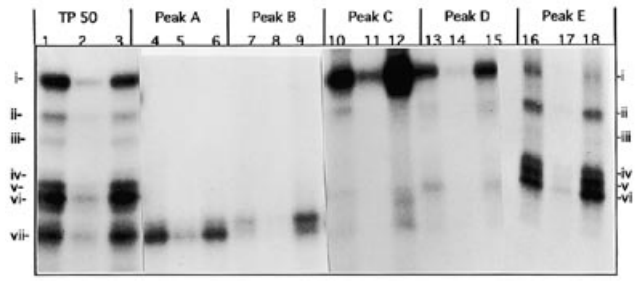

Figure 8. SDS–PAGE analysis of RP-HPLC fractions containing p*2674–2653HHABA-labeled 50S proteins. Autoradiogram of SDS–PAGE analysis of labeled TP50 (lanes 1–3) and of RP-HPLC peaks A (lanes 4–6), B (lane 7–9), C (lanes 10–12), D (lanes 13–15) and E (lanes 16–18). Lanes 1, 4, 7, 10, 13 and 16 are peaks from 50S subunits labeled by p*2674–2653HHABA in the absence of added cDNAs; lanes 2, 5, 8, 11, 14 and 17 are peaks from 50S subunits labeled by p*2674–2653HHABA in the presence of added cDNA 2674–2652; lanes 3, 6, 9, 12, 15 and 18 are peaks from 50S subunits labeled by p*2674–2653HHABA in the presence of added MM-cDNA 2674–2652. Bands indicated to the left and right of the gel correspond to labeled proteins in lanes 1 and 18 respectively.

RNase H hydrolysis within a given cDNA:RNA heteroduplex (24). The labeled 160 nt fragment seen in Figure 5B, lane 4 demonstrates that the major site of photoincorporation occurs between nt 2497–2505 and the target site for probe binding, nt 2653–2674. A minor site of photoincorporation falling between nt 2653–2674 and the 3′-terminus is indicated by the presence of the labeled fragment of ~260 nt in lanes 2–4. This latter site was further localized to between nt 2653–2674 and 2731–2740 by the presence of the ~83 nt band in Figure 5C, lane 3, as well as the absence of a band of ~190 nt (nt 2740–2904) in this same lane. In an effort to determine whether there were other significant sites of photoincorporation in 23S rRNA, similar experiments were also performed adding 23S rRNA-complementary cDNA probes 578–569, 811–803, 1060–1051, 1400–1391, 1750–1741 and 2310–2301 to labeled 23S rRNA, one at a time or in pairs. No additional photoincorporation sites were found.

Specific sites of photoincorporation within the region nt 2497–2904 were identified by reverse transcriptase primer extension (24) on 23S rRNA extracted from 50S subunits photolabeled by 2674–2653HHABA (Fig. 6). Stops or pauses dependent on the presence of covalently bound 2674–2653HHABA are seen both upstream of and within the target binding site. The strong stops seen at U2653 and A2654 presumably reflect photoincorporation into nt C2652 and U2653, immediately adjacent to the site of generation of the nitrene opposite A2654. A strong stop is also visible at A2670, reflecting incorporation into G2669. The stops indicating minor amounts of incorporation near and between these sites may be due to reverse transcriptase ‘stuttering’ around the major sites of photoincorporation (36). Minor but reproducible stops were also seen at positions G2633 and A2634, reflecting minor photoincorporation into A2632 and G2633.

Table 2. SDS–PAGE analysis of specificially labeled RP-HPLC peaks

RP-HPLC peak[a]	Bands[b]	Apparent mass (kDa)[c]	Labeled protein[d]	Apparent mass of unlabeled protein (kDa)[c]	Calculated mass of unlabeled protein (kDa)[e]
A	vii	17.8	L27	11.0	9.0
B	vi-a	19.0	L24	12.5	11.2
C	i	39.5	L2	29.7	29.8
D	**i**	39.5	L2	29.7	29.8
	v-a	22.4	L17	13.3	14.4
E	i	39.5	L2	29.7	29.8
	ii	33.5	L1	24.6	24.6
	iii	29.0	L5	20.2	20.2
	iv	24.6	L9	15.0	15.7
	v	23.0	L15/16	14.5	15.0/15.3
	vi	21.7	L15/16	14.5	15.0/15.3

[a]See Figure 7.
[b]In the case of multiple bands that in bold is most intense.
[c]Calculated from migration on SDS–PAGE analysis, using a standard curve of electrophoretic migration distance versus log molecular mass.
[d]See Results and Figure 9.
[e]Giri *et al*. (37).

Proteins site-specifically labeled on photolysis of the 50S–p*2674–2653HHABA complex

Site-specifically labeled proteins were for the most part identified by combining RP-HPLC and SDS–PAGE analyses. When this combination proved insufficient, agarose antibody affinity chromatography was used in addition.

RP-HPLC analysis of TP50 extracted from labeled 50S gave a total of five site-specifically labeled peaks, A–E, as evidenced by the strong reduction in labeling seen for complexes prepared in the presence of competing cDNA but not in the presence of MM-cDNA (Fig. 7). Fractions corresponding to these peaks were pooled and analyzed by SDS–PAGE and autoradiography (Fig. 8). We have previously shown that ribosomal proteins covalently labeled with oligoDNAs elute on RP-HPLC with or close to unmodified protein and migrate in SDS–PAGE with apparent masses approximately equal to the sum of the masses of the labeled protein and of the attached oligoDNA (22–26), which in this case is 7.4 kDa.

SDS–PAGE analysis of labeled TP50 revealed the presence of at least seven labeled bands, denoted i–vii (Fig. 8). Such analysis was also performed on RP-HPLC fractions corresponding to peaks A–E (Fig. 8). The results, summarized in Table 2, were sufficient to identify L1, L2, L5, L9, L15, L16, L27 and L24 (band vi-a, falling between bands vi and vii) as site-specifically labeled proteins. Confirmation that band Dv-a (migrating between bands v and vi) corresponds to labeled protein L17 was provided by agarose antibody affinity chromatography analysis (Fig. 9). Labeled L1, identified as band Eii, elutes over a broad range and is also observed in the fractions eluting with unmodified L1 (data not shown). A broad peak of labeled L1 elution was earlier observed with another oligoDNA probe (25). The minor band iii, corresponding to labeled L5, is only observed in peak E and several fractions following it.

Considering the intensities of the RP-HPLC peaks and the SDS–PAGE autoradiographic bands, protein L2 is clearly the most highly labeled protein, L1, L15, L16 and L27 can be classified as intermediate labeled proteins and L5, L9, L17 and L24 are each labeled to a minor extent.

DISCUSSION

The present results clearly demonstrate that a cDNA complementary to the loop and 3′-stem of the α-sarcin region is capable of forming a complex with its target site in isolated 50S subunits, similar to what has been found by two other groups (28,38) for 70S ribosomes. Our results are consistent with the observation of Meyer *et al*. (28) that cDNAs complementary to the α-sarcin loop do not affect association or dissociation of 70S subunits; if binding were much stronger to 70S ribosomes as against 50S subunits then addition of cDNA should have favored association.

The direct evidence for cDNA 2674–2652 and p*2674–2653HHABA binding to the target site is based on three different experimental results. First, probe-induced changes in 23S rRNA methylation within the 50S subunit are only found at or adjacent to the target site (Fig. 4). Second, the major sites of labeling of 23S rRNA on photolysis of the 50S–p*2674–2653HHABA complex are at or just outside the target site (Fig. 6). Third, labeling by p*2674–2653HHABA of 23S rRNA and of each of the proteins indicated is markedly reduced when the 50S complex to be photolyzed is formed in the presence of competing non-photolabile,

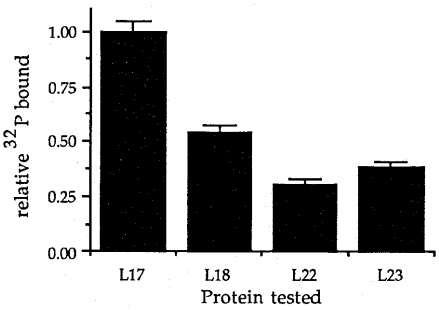

Figure 9. Agarose antibody affinity chromatography analysis of RP-HPLC peak D.

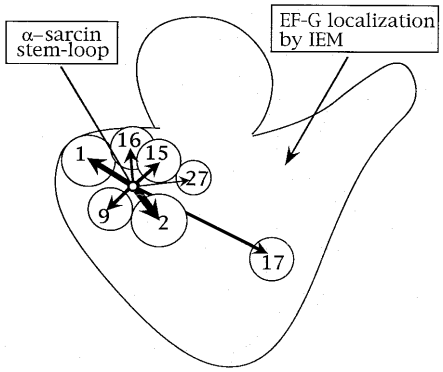

Figure 10. Localization of the α-sarcin loop of 23S rRNA within the 50S subunit. The placement of labeled proteins L1, L2, L5, L9, L15, L17 and L27 follows the model of Walleczek *et al*. (39). The placement of L16 is according to Nag *et al*. (41). Protein L24 has not been placed.

non-radioactive cDNA 2674–2652. In contrast, such labeling is not appreciably affected when MM-cDNA 2674–2652, which should bind much more weakly if at all to the target site, is present during complex formation (Figs 7 and 8). We thus conclude that portions of nine proteins L1, L2, L15, L16 and L27 (major or intermediate labeled proteins) and L5, L9, L17 and L24 (minor labeled proteins) all lie within 23 Å of nt U2653 of 23S rRNA in 50S subunits.

There are two caveats to this conclusion. First, hybridization of 2674–2653HHABA to the 50S subunit clearly causes at least local perturbation (Fig. 4), so that our results do not reflect the native 50S structure. Because of the current low resolution of the structural model for this particle, this is not a major concern. Second, only 20% of the 50S subunits bind probe with high affinity and by our protocol we are measuring photoincorporation essentially exclusively from this population, which might not be representative of 'active' ribosomes. We think this possibility remote, given the consistency of our results with other measures of 50S protein placement (*vide infra*).

Labeled proteins L1, L2, L9, L15 and L27 are proximal to one another, near the L1 projection, in the 50S protein placement model of Walleczek *et al*. (39), which was derived from cross-linking and immunoelectron microscopy (IEM) results. In addition, L5 forms part of the central protruberance of the 50S subunit and is also near the L1 projection (40) and L16 is located at the base of the L1 projection (41). We thus conclude that U2653 is at or near the epicenter of these proteins, as depicted in Figure 10. Labeling of L17 is the only apparent inconsistency between our results and the Wallaczek *et al*. model. In support of moving L17 closer to the L1 projection, we note that Kenny and Traut (42) have reported an L2–L17 crosslink and that L17 is linked to proteins L2, L15, L16 and L27 in the 50S assembly map (43).

Placement of the α-sarcin region at the base of the L1 projection puts it quite far from the site of EF-G and EF-Tu binding, localized by IEM near the L7/L12 stalk (44,45; see Fig. 10). Naively one would have expected closer proximity, since these factors protect nucleotides in the α-sarcin loop from chemical modification (9) and EF-G protects the loop from α-sarcin cleavage (10). However, as shown by X-ray crystallography (46,47), EF-G is a very elongated molecule, with a longest dimension of ~118 Å. Our results may therefore be interpreted as indicating that when EF-G binds to the 50S subunit it spans the distance between the base of the L7/L12 stalk and the base of the L1 projection.

Our protein cross-linking results also allow us to draw conclusions regarding the placement of the α-sarcin loop, located in domain VI, relative to other regions of 23S rRNA. Of the proteins labeled by p*2674–2653HHABA, L2, L15, L16 and L27 are at or near the peptidyl transferase center (48) and L2 appears to have a functional role in this activity (49,50). Since the RNA portion of the peptidyl transferase center has been localized to the central loop of domain V (51,52) and L2 binding to 23S rRNA has been localized to two nucleotide sequences within domain IV (53), our results provide direct evidence for the proximity of the α-sarcin region to domains IV and V. Additional evidence for this conclusion comes from our earlier result demonstrating that a photolabile cDNA probe targeted to nt 2497–2505 in the central loop of domain V cross-links to L3 (23), which binds to rRNA in domain VI (53). Recent tRNA localization experiments by Joseph and Noller (54) further demonstrate the mutual proximity of domains IV, V and VI within the 50S subunit. In this study Fe(II)-EDTA attached to the 5′-end of A site-bound tRNA induced hydroxyl radical cleavages within the α-sarcin loop (domain VI), within the 2550 loop in domain V and between nt 1940–1965, abutting one of the L2 binding sites (nt 1971–1989) in domain IV. Finally, two of the nine proteins labeled by p*2674–2653HHABA, L15 and L17, are also labeled by a cDNA probe targeted to nt 803–811 in domain II (55), suggesting the proximity of the α-sarcin region to this domain.

In conclusion, the work reported in this paper allows us to define the protein environment within 23 Å of U2653 in 23S rRNA and to localize the α-sarcin loop at or near the base of the L1 projection. These and related results suggest a central and functionally important location for this loop within the 50S subunit, proximal to portions of 23S rRNA domains II, IV and V. Such a location provides a compelling rationale for the extreme sensitivity of ribosomal function to sarcin-catalyzed cleavage within the α-sarcin loop.

ACKNOWLEDGEMENTS

We acknowledge with thanks the excellent technical assistance of Ms Nora Zuño in several aspects of this work and Dr Richard Brimacombe for carrying out the agarose antibody affinity chromatography analyses. This work was supported by NIH grant GM-53416 and NSF grant MCB-9118072.

REFERENCES

1 Sacco,G., Drickamer,K. and Wool,I.G. (1983) *J. Biol. Chem.*, **258**, 5811–5818.
2 Wool,I.G. (1984) *Trends Biochem. Sci.*, **9**, 14–17.
3 Endo,Y., Mitsui,K., Motizuki,M. and Tsurugi,K. (1987) *J. Biol. Chem.*, **262**, 5908–5912.
4 Endo,Y. and Wool,I.G. (1982) *J. Biol. Chem.*, **257**, 9054–9060.
5 Szewczak,A.A., Moore,P.B., Chan,Y.-L. and Wool,I.G. (1993) *Proc. Natl. Acad. Sci. USA*, **90**, 9581–9585.
6 Leffers,H., Egebjerg,J. Andersen,A., Christensen,T. and Garrett,R.A. (1988) *J. Mol. Biol.*, **204**, 507–522.
7 Fernandez-Puentes,C. and Vazquez,D. (1977) *FEBS Lett.*, **78**, 143–146.
8 Hausner,T.-P., Atmadja,J. and Nierhaus,K. (1987) *Biochimie*, **69**, 911–923.
9 Moazed,D., Robertson,J.M. and Noller,H.F. (1988) *Nature*, **334**, 362–364.
10 Miller,S.P. and Bodley,J.W. (1991) *Nucleic Acids Res.*, **19**, 1657–1660.
11 Tapprich,W.E. and Dahlberg,A.E. (1990) *EMBO J.*, **6**, 4235–4239.
12 Tapio,S. and Isaksson,L.A. (1991) *Eur. J. Biochem.*, **202**, 981–984.

13 Melançon,P., Tapprich,W.E. and Brakier-Gingras,L. (1992) *J. Bacteriol.*, **174**, 7896–7901.
14 Bilgin,N. and Ehrenberg,M. (1994) *J. Mol. Biol.*, **235**, 813–824.
15 Wool,I.G., Glück,A and Endo,Y. (1992) *Trends Biochem. Sci.*, **17**, 266–269.
16 Nierhaus,K.H., Schilling-Baretzko,S. and Twardowski,T. (1992) *Biochimie*, **74**, 403–410.
17 Glück,A., Endo,Y. and Wool,I.G. (1994) *Nucleic Acids Res.*, **22**, 321–324.
18 Szewczak,A.A. and Moore,P.B. (1995) *J. Mol. Biol.*, **247**, 81–98.
19 Glück,A and Wool,I.G. (1996) *J. Mol. Biol.*, **256**, 838–848.
20 Liu,R. and Liebman,S.W. (1996) *RNA*, **2**, 254–263.
21 O'Connor,M. and Dahlberg,A.E. (1996) *Nucleic Acids Res.*, **24**, 2701–2705.
22 Cooperman,B., Muralikrishna,P. and Alexander,R.W. (1993) In Nierhaus,K.H., Subramanian,A.R., Erdmann,V.A., Franceschi,F. and Wittman-Liebold,B. (eds), *The Translational Apparatus.* Plenum Press, New York, NY, pp. 465–476.
23 Alexander,R.W., Muralikrishna,P. and Cooperman,B.S. (1994) *Biochemistry*, **33**, 12109–12118.
24 Muralikrishna,P. and Cooperman,B.S. (1991) *Biochemistry*, **30**, 5421–5428.
25 Muralikrishna,P. and Cooperman,B.S. (1994) *Biochemistry*, **33**, 1392–1398.
26 Muralikrishna,P. and Cooperman,B.S. (1995) *Biochemistry*, **34**, 115–121.
27 Brimacombe,R. (1995) *Eur. J. Biochem.*, **230**, 365–383.
28 Meyer,H.A., Triana-Alonso,F., Spahn,C.M., Twardowski,T., Sobkiewicz,A. and Nierhaus,K.H (1996) *Nucleic Acids Res.*, **24**, 3996–4002.
29 Sambrook,J., Fritsch,E.F. and Maniatis,T. (1989) *Molecular Cloning: A Laboratory Manual*, 2nd Edn. Cold Spring Harbor Laboratory Press, Cold Spring Harbor, NY, pp. 11–39.
30 Kerlavage,A.R. and Cooperman,B.S. (1986) *Biochemistry*, **25**, 8002–8010.
31 Kerlavage,A.R., Weitzmann,C.J. and Cooperman,B.S. (1984) *J. Chromatogr.*, **317**, 201–212.
32 Gulle,H., Hoppe,E., Osswald,M., Greuer,B., Brimacombe,R. and Stöffler,G. (1988) *Nucleic Acid Res.*, **16**, 815–832.
33 Henderson,E. and Lake,J.A. (1985) In *Proceedings of the 16th FEBS Congress*, Part B. VNU Science Press, London, pp 219–228.
34 White,G.A., Wood,T. and Hill,W.E. (1988) *Nucleic Acids Res.*, **16**, 10817–10831.
35 Egebjerg,J., Larsen,N. and Garrett,R.A. (1990) In Hill,W.E., Dahlberg,A., Garrett,R.A., Moore,P.B., Schlessinger,D. and Warner,J.R. (eds), *The Ribosome: Structure, Function and Evolution*. American Society for Microbiology, Washington, DC, pp. 168–179.
36 Denman,R., Colgan,J., Nurse,K. and Ofengand,J. (1988) *Nucleic Acids Res.*, **16**, 165–178.
37 Giri,L., Hill,W.E. and Wittmann,H.G. (1984) *Adv. Protein Chem.*, **36**, 1–78.
38 Hill,W.E., Bucklin,D.J., Bullard,J.M., Galbraith,A.L., Jammi,N.V., Rettberg,C.C., Sawyer,B.S. and van Waes,M.A. (1995) *Biochem. Cell Biol.*, **73**, 1033–1039.
39 Wallazcek,J., Schuler,D., Stöffler-Meilicke,M., Brimacombe,R. and Stöffler,G. (1988) *EMBO J.*, **7**, 3571–3576.
40 Nag,B., Tewari,D.S., Sommer,A., McKuskie-Olson,H., Glitz,D.G. and Traut,R.R.(1987) *J. Biol. Chem.*, **262**, 9681–9687.
41 Nag,B., Glitz,D.G., Tewari,D.S. and Traut,R.R. (1991) *J. Biol. Chem.*, **266**, 11116–11121.
42 Kenny,J.W. and Traut,R.R. (1979) *J. Mol. Biol.*, **127**, 243–263.
43 Herold,M. and Nierhaus,K.H. (1987) *J. Biol. Chem.*, **262**, 8826–8833.
44 Girshovich,A.S., Kurtskhalia,T.V., Ovchinnikov,Y. and Vasiliev,V.D. (1981) *FEBS Lett.*, **130**, 54–59.
45 Girshovich,A.S., Bochkareva,E.S. and Vasiliev,V.D. (1986) *FEBS Lett.*, **197**, 192–198.
46 Aevarsson,A., Brazhnikov,E., Garber,M., Zheltonosova,J., Chirgadze,Y., al-Karadaghi,S., Svensson,L.A. and Liljas,A. (1994) *EMBO J.*, **13**, 3669–3677.
47 Czworkowski,J., Wang,J., Steitz,T.A. and Moore,P.B. (1994) *EMBO J.*, **13**, 3661–3668.
48 Cooperman,B.S., Weitzmann,C.J. and Fernandez,C.L. (1990) In Hill,W.E., Dahlberg,A., Garrett,R.A., Moore,P.B., Schlessinger,D. and Warner,J.R. (eds), *The Ribosome: Structure, Function and Evolution*. American Society for Microbiology, Washington, DC, pp. 491–501.
49 Wooten,T.L. (1996) PhD Thesis in Chemistry, University of Pennsylvania, Philadelphia, PA.
50 Cooperman,B.S., Wooten,T., Romero,D.P. and Traut,R.R. (1995) *Mol. Cell. Biol.*, **74**, 1087–1094.
51 Porse,B.T and Garrett,R.A. (1995) *J. Mol. Biol.*, **249**, 1–10.
52 Garrett,R.A. and Rodriguez-Fonseca,C. (1996) In Zimmermann,R.A. and Dahlberg,A. (eds), *Ribosomal RNA: Structure, Evolution, Processing and Function*. CRC Press, Boca Raton, FL, pp. 327–355.
53 Egebjerg,J., Christiansen,J. and Garrett,R.A. (1991) *J. Mol. Biol.*, **222**, 251–264.
54 Joseph,S. and Noller,H.F. (1996) *EMBO J.*, **15**, 910–916.
55 Alexander,R.W. and Cooperman,B.S. (1997) *Biochemistry*, submitted for publication.